Spin Pumping Driven by Magnon Polarons

Hiroki Hayashi and Kazuya Ando*
Department of Applied Physics and Physico-Informatics, Keio University, Yokohama 223-8522, Japan

(Received 16 May 2018; revised manuscript received 12 October 2018; published 4 December 2018)

We report the observation of a resonant enhancement of spin pumping induced by magnon-phonon coupling at room temperature. We show that the spin pumping driven by microwave parametric excitation is enhanced, compared to its purely magnonic value, when the microwave excites dipole-exchange magnons in the proximity of the intersection of the uncoupled magnon and phonon dispersions. This observation is consistent with a model of the spin pumping driven by hybridized magnon-phonon modes, magnon polarons, where the spin-pumping efficiency depends on the relative scattering strengths of the magnons and phonons in a magnetic insulator.

DOI: 10.1103/PhysRevLett.121.237202

The coupled dynamics of magnetic and lattice waves (magnons and phonons) was first investigated more than half a century ago [1]. The coupling between magnons and phonons stems from spin-orbit, dipole-dipole, and exchange interactions in magnetic crystals [2]. The strength of this coupling is maximized in the proximity of the intersection of the uncoupled magnon and phonon dispersions (see Fig. 1). In the intersection region, the normal modes of the system are no longer either purely magnetic or elastic, but are admixtures of both properties; the coupling gives rise to the formation of hybridized magnon and phonon modes, called magnon polarons [3,4].

Although the magnon-phonon coupling can often be ignored, this coupling has recently been shown to play a crucial role in spintronic and magnonic phenomena [6–9]. Recent experimental and theoretical studies have revealed that the spin Seebeck effect (SSE), the generation of a spin current as a result of a temperature gradient, can be enhanced or suppressed by the magnon-phonon coupling, depending on the relative scattering strengths of the magnons and phonons in a magnetic insulator [10,11]. The hybridization also plays an essential role in the thermalization of parametrically excited magnons; an accumulation of magnon polarons in the spectral region near the intersection has been observed [12]. More recently, the direct evidence of spin transfer from coherent magnons generated by a microwave into phonons has been obtained from wave-vector-resolved Brillouin light scattering [13]. These findings shed new light on the magnon-phonon coupling, leading to a revival of interest in the coupled dynamics of magnetic and lattice waves [8,14–16].

In this Letter, we report the observation of a resonant enhancement of the spin pumping induced by the magnon-phonon coupling. The spin pumping refers to the generation of a spin current from dynamical magnetization [17–34]. We demonstrate that a spin current pumped from a magnetic insulator $Y_3Fe_5O_{12}$ (YIG) shows an anomaly under microwave parametric pumping. The parametric pumping process involves the splitting of microwave photons from the pumping microwave into pairs of magnons with one-half of the pumping frequency, $f_p/2$, and oppositely oriented wave vectors $\mathbf{k} \neq \mathbf{0}$ through the virtual excitation of the uniform magnons with f_p, as shown in Fig. 1 [2]. The wave vector of the parametric magnons can be tuned by shifting the magnon dispersion in the momentum-frequency space using an external magnetic field.

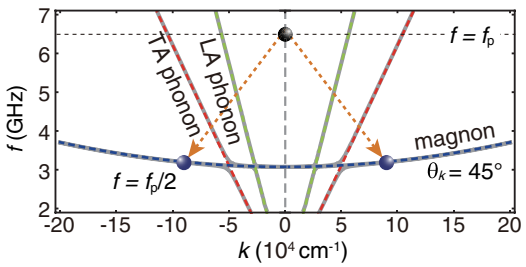

FIG. 1. Schematic dispersions of magnons (the dashed curve in blue), transverse-acoustic (TA) phonons (the dashed line in red), and longitudinal-acoustic (LA) phonons (the dashed line in green) in a YIG film with anticrossings due to the magnon-phonon coupling, where f and k are the frequency and wave number. The magnon dispersion was calculated for $\theta_k = 45°$, where θ_k is the angle between $\mathbf{k}$ and $\mathbf{H}$. A schematic of the microwave parametric pumping is also shown; a $\mathbf{k} = \mathbf{0}$ uniform-mode magnon (the black circle) with the frequency of f_p is excited virtually, or nonresonantly, and splits into a pair of magnons (the blue circles) with the frequency of $f_p/2$ and opposite wave vectors $\mathbf{k} \neq \mathbf{0}$. The wave number of the intersection of the uncoupled magnon and LA phonon dispersions is so small that the magnons with this wave number cannot be excited by the parametric pumping. The dispersion of the optical phonons is not shown because the energy of the optical modes is in the THz range [5], far above the energy of the parametrically excited magnons.

We found that the anomaly in the spin pumping appears when the microwave parametric pumping excites dipole-exchange magnons in the proximity of the intersection of the uncoupled magnon and phonon dispersions at room temperature. This feature is critically different from the SSE. In the SSE, the magnon-polaron contribution is pronounced at low temperatures and is observed only when the magnon and phonon modes are coupled over a large volume in momentum space [10]. The reason for this difference is that the SSE is driven by thermally generated magnons with a wide range of frequencies and wave vectors [35], whereas the microwave spin pumping is driven by magnons with a narrow range of frequencies and wave vectors. Owing to the controllability of the magnon modes responsible for the spin-current generation, the magnon-polaron spin pumping promises a way to study the physics of the magnon-phonon coupling and magnon polarons in magnetic insulators.

We study the perpendicular parametric spin pumping in a Pt (7.5 nm)/YIG (28 μm) bilayer film, where the numbers in parentheses represent the thickness. The single-crystalline YIG (111) film was grown by a liquid phase epitaxy on a $Gd_3Ga_5O_{12}$ (111) substrate (a 2×2 mm square shape). On the surface of the YIG film, the Pt layer was sputtered in an Ar atmosphere. The Pt/YIG film was placed on a coplanar waveguide, where a microwave was applied to the input of the signal line as show in Fig. 2(a). The signal line is 160 μm wide, and the gaps between the signal line and the ground lines were designed to match to the characteristic impedance of 50 Ω. An in-plane external magnetic field $\mathbf{H}$ was applied parallel to the signal line. Under the magnetic resonance condition, the microwave creates nonequilibrium magnons in the YIG layer, which drive the spin pumping. The spin pumping injects a spin current in to the Pt layer, and the spin current is converted into an electric voltage V_{ISHE} through the inverse spin Hall effect (ISHE) in the Pt layer [21]. To measure the spin current emitted from the YIG layer using the ISHE, two electrodes were attached to the edges of the Pt layer. All the measurements were performed at room temperature.

Figure 2(b) shows $\mu_0 H$ dependence of the microwave absorption intensity P_{abs} and voltage V_{ISHE} signals measured with applying a microwave with a frequency of $f_{\mathrm{p}} = 6.5$ GHz and a power of $P = 50$ and 250 mW. This result shows that the ferromagnetic resonance (FMR) is excited around $\mu_0 H = 140$ mT, where we observed the voltage signals V_{ISHE} due to the ISHE induced by the spin pumping. At $P = 50$ mW, we observed only the P_{abs} and V_{ISHE} signals due to the excitation of the FMR and magnetostatic spin waves around $\mu_0 H = 140$ mT [37]. By increasing the microwave power from $P = 50$ to 250 mW, additional P_{abs} and V_{ISHE} signals appear far below the FMR field (40 mT $< \mu_0 H <$ 100 mT). These P_{abs} and V_{ISHE} signals are generated by the parametric pumping; the voltage is generated by the ISHE due to the spin pumping

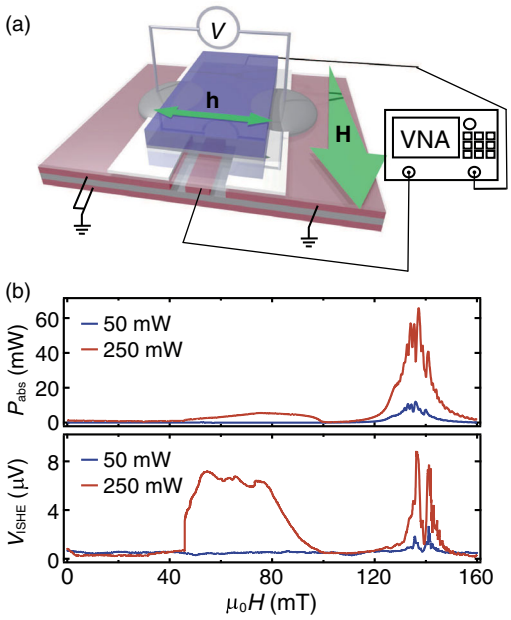

FIG. 2. (a) A schematic illustration of the experimental setup, where $\mathbf{H}$ is the external magnetic field and $\mathbf{h}$ is the microwave magnetic field. The microwave absorption intensity P_{abs} in the Pt/YIG film was determined by measuring S_{21} using a vector network analyzer (VNA): $P_{\mathrm{abs}} = (\Delta|S_{21}|^2/|S_{21}^0|)P_{\mathrm{in}}$, where $|S_{21}^0|$ represents the ratio between the incident and transmitted microwave power without the parametric excitation. $\Delta|S_{21}|^2$ is the change ratio of the transmitted microwave power [36]. (b) Magnetic field H dependence of the microwave absorption intensity P_{abs} and ISHE voltage V_{ISHE} measured at the microwave frequency of $f_{\mathrm{p}} = 6.5$ GHz with the power of $P = 50$ mW (the solid curve in blue) and 250 mW (the solid curve in red).

driven by parametrically excited magnons [29], pairs of magnons with the frequency of $f_{\mathrm{p}}/2$ and opposite wave vectors $\mathbf{k} \neq \mathbf{0}$ [45] (see also Fig. 1). In Figs. 3(a) and 3(b), we show the $\mu_0 H$ dependence of P_{abs} and V_{ISHE} induced by the parametrically excited magnons measured at various excitation powers P.

The difference in the spectral shape of P_{abs} and V_{ISHE}, shown in Figs. 3(a) and 3(b), is due to the wave-vector-dependent spin-pumping efficiency of the parametric magnons [46]. To characterize the spin-pumping efficiency, we plot $\kappa \equiv V_{\mathrm{ISHE}}/P_{\mathrm{abs}}$ in Fig. 3(c). Figure 3(c) shows that κ changes systematically with $\mu_0 H$. At each P, κ jumps abruptly at a certain field with increasing $\mu_0 H$. The field where κ jumps corresponds to the field where the dominant magnon mode switches from the exchange to the dipole-exchange modes [46]. Here, the wave number of the primary magnons excited by the parametric excitation varies with $\mu_0 H$ [47]. At low $\mu_0 H$, only exchange magnons with $k \sim 10^5$ cm^{-1} can be excited, because no states of dipole-exchange magnons are available at $f_{\mathrm{p}}/2$. By increasing $\mu_0 H$, the magnon dispersion shifts in momentum-frequency space, and above a certain field, dipole-exchange magnons with $k \sim 10^3$–10^4 cm^{-1} can be excited. Figure 3(c) shows that the

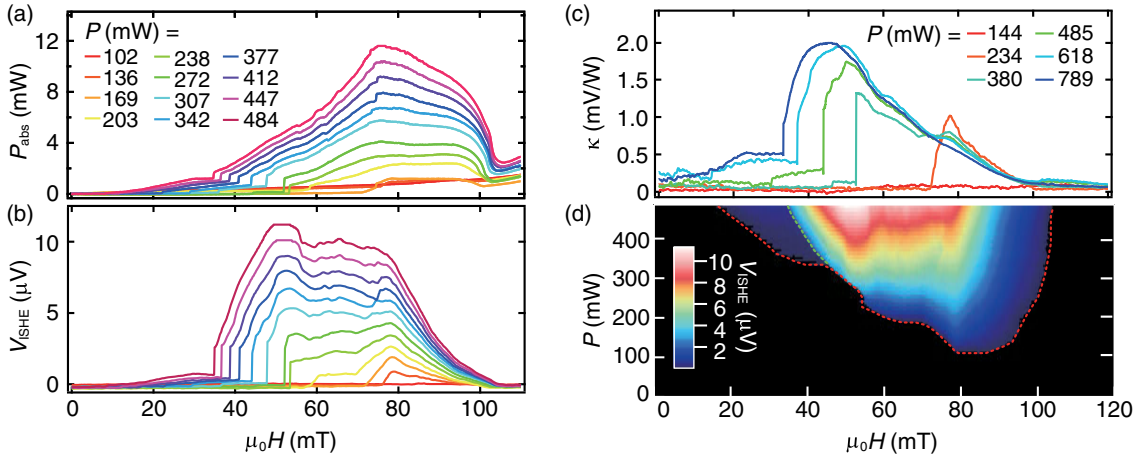

FIG. 3. (a) Magnetic field H dependence of the microwave absorption intensity P_{abs} measured at $f_p = 6.5$ GHz with various excitation powers P. (b) H dependence of the ISHE voltage V_{ISHE} measured at $f_p = 6.5$ GHz with various P. (c) H dependence of the spin-pumping efficiency $\kappa = V_{ISHE}/P_{abs}$ at $f_p = 6.5$ GHz with various P. (d) The two-dimensional plot of V_{ISHE} as a function of $\mu_0 H$ and P. The dashed curve in red denotes the threshold power of the parametric excitation.

switching field depends on P, which can be attributed to the above threshold effect [46]. We also note that because of the higher threshold power of the parametric excitation of the exchange magnons, only the dipole-exchange magnons are excited at $P = 234$ mW.

Figure 3(c) shows that an anomaly appears in the spin-pumping efficiency of the dipole-exchange magnons. The overall feature of the result shown in Fig. 3(c) is that κ decreases with $\mu_0 H$ above the field where κ jumps ($\mu_0 H > 40$–50 mT). In the decreased part of κ, where the dipole-exchange magnons are excited, the magnitude of κ is almost independent of P, which is consistent with the spin-pumping efficiency of the dipole-exchange magnons [46]. It is notable that a peak signal appears in the spin-pumping efficiency κ at $\mu_0 H = 78$ mT, as shown in Fig. 3(c).

The enhanced spin-pumping efficiency κ at $\mu_0 H = 78$ mT originates from the magnon-phonon coupling in the Pt/YIG bilayer. To identify the wave vector of the magnons excited around $\mu_0 H = 78$ mT, we have calculated the $\mu_0 H$ dependence of the primary excited magnons at the threshold power by finding k and θ_k that minimize the parametric pumping threshold $h_{th}(\mathbf{k}) = \gamma_\mathbf{k}/V_\mathbf{k}$ using the coupled lateral mode theory with the measured threshold shown in Fig. 3(d) [48]. Here, θ_k is the angle between $\mathbf{k}$ and $\mathbf{H}$, $\gamma_\mathbf{k}$ is the damping of the magnon with the momentum $\hbar\mathbf{k}$, and $V_\mathbf{k}$ is the coupling strength between the uniform-mode and a pair of $\pm\mathbf{k}$ magnons. Figure 4(a) shows the field dependence of k and θ_k calculated using the saturation magnetization $\mu_0 M_s = 175$ mT and the exchange stiffness constant $D = 1.05 \times 10^{-5}$ m^2/s for the YIG film [46]. This result shows that the dipole-exchange magnons with $k \simeq 5.25 \times 10^4$ cm^{-1} and $\theta_k \simeq 45°$ are primary excited by the parametric pumping at $\mu_0 H = 78$ mT. Using the result shown in Fig. 4(a), we show a schematic of the primary excited mode and the dispersions of magnons and transverse-acoustic (TA) phonons in Fig. 4(b). This result shows that only near $\mu_0 H = 78$ mT, the parametric pumping creates magnons at the intersection of the uncoupled magnon and phonon dispersions, showing that the peak of κ

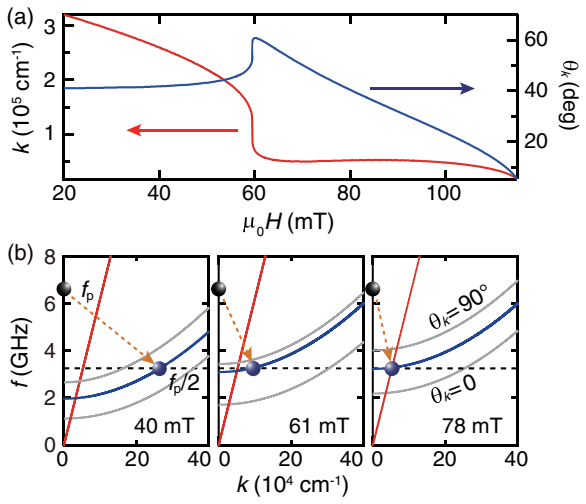

FIG. 4. (a) The calculated $\mu_0 H$ dependence of the wave number k, and the angle θ_k between $\mathbf{k}$ and $\mathbf{H}$ of the parametrically-excited magnons under the $f_p = 6.5$ GHz microwave application. The calculated curves were obtained using $\mu_0 M_s = 175$ mT, $B/A = 2.55$, and $k_c = 8.5 \times 10^7$ m^{-1} (for details, see Ref. [48]). (b) Schematic dispersions of magnons (the curve in blue) and TA phonons (the line in red) in a YIG film at $\mu_0 H = 40$, 61, and 78 mT. A schematic of the uniform-mode magnon (the black circle) with the frequency of f_p and wave number $k = 0$ and the parametrically excited magnon (the blue circles) with the frequency of $f_p/2$ and nonzero wave number $k \neq 0$ is also shown. The highest and lowest branches of the magnon dispersion are also shown (the curves in gray).

is associated with the magnon-phonon coupling. The calculated magnon dispersion at $\mu_0 H = 78$ mT also shows that the peak of κ is irrelevant to the enhanced spin pumping due to the three-magnon process [37,49,50]. Here, the peak linewidth of κ is around 10 mT [see Fig. 3(c)]. The main reason for the relatively large linewidth is that the wave number k_p of the primary excited parametric magnons changes only slightly with $\mu_0 H$ in the dipole-exchange region, as shown in Fig. 4(a). Within the peak linewidth, the change of the wave number is only around 0.3×10^4 cm^{-1}, which is more than an order of magnitude smaller than the wave number of the possible hybridized magnon-phonon mode, $k_{mp} = 5.25 \times 10^4$ cm^{-1}. We note that the magnons excited close to the intersection still possess the hybridization character, even though the hybridization effect is suppressed by departing from the intersection point. The range of the wave number $k_{mp} \pm \Delta k_{mp}$ where the hybridization character is present depends on the strength of the magnon-phonon coupling, and Δk_{mp} can be around 0.1×10^4 cm^{-1} [51]. We also note that although the parametric pumping excites magnons with a narrow range of wave vectors and energies, the wave vector and energy are known to be spread slightly by the four-magnon scattering [52]. Because the range of the wave number of the pumped magnons within the peak linewidth is comparable to the range of the wave number where the magnon-phonon coupling plays a role, the magnon-polaron spin pumping can be driven in the relatively large magnetic field range.

The magnetic field where the peak of κ appears changes systematically with the microwave pumping frequency f_p, which further evidences that the magnon polarons are responsible for the enhanced spin pumping. In Figs. 5(a) and 5(b), we show the normalized spin-pumping efficiency $\bar{\kappa} \equiv \kappa(\mu_0 H)/\kappa(\mu_0 H = 60\ \text{mT})$ measured at $f_p = 6.0$ and 6.5 GHz, respectively. Both results show that the peak of the spin-pumping efficiency is suppressed by increasing the excitation power P, which can be attributed to nonlinear limiting mechanisms above the threshold of the parametric excitation, such as the nonlinear damping and dephasing mechanisms [2]; the nonlinear damping mechanism refers to the nonlinear increase of the damping of the excited modes due to magnon-magnon interactions, such as the four-magnon interaction, and the phase mechanism refers to the disappearance of the phase correlation between the pumping and the excited magnons due to the nonlinear interaction between the magnons. Figures 5(a) and 5(b) further demonstrate that the magnetic field where the peak of $\bar{\kappa}$ appears at $f_p = 6.0$ GHz is lower than that at $f_p = 6.5$ GHz. To quantitatively discuss the f_p dependence of the anomaly in the spin-pumping efficiency, we show H dependence of $\Delta\bar{\kappa} \equiv \bar{\kappa}(P) - \bar{\kappa}(P = 800\ \text{mT})$ in Fig. 5(c), where the purely magnonic spin-pumping efficiency is subtracted from $\bar{\kappa}$. We define the magnetic field where $\Delta\bar{\kappa}$ is maximized as H_{peak}.

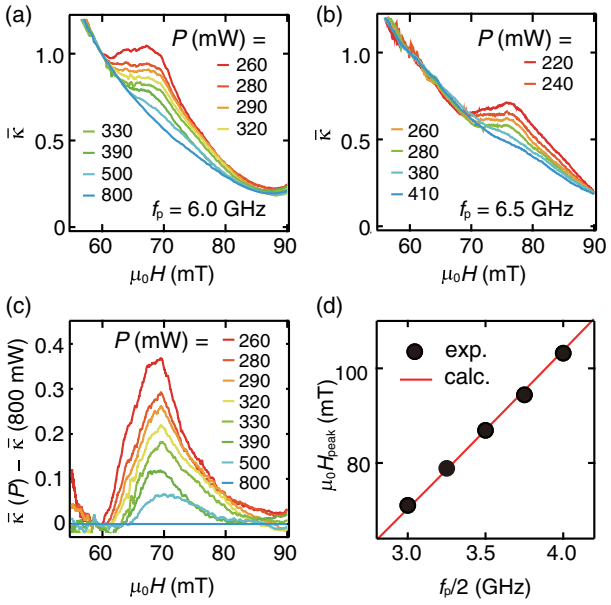

FIG. 5. (a) Magnetic field H dependence of the normalized spin-pumping efficiency $\bar{\kappa} \equiv \kappa(\mu_0 H)/\kappa(\mu_0 H = 60\ \text{mT})$ at $f_p = 6.0$ GHz with various P. (b) H dependence of $\bar{\kappa}$ at $f_p = 6.5$ GHz with various P. (c) H dependence of $\bar{\kappa}(P) - \bar{\kappa}(P = 800\ \text{mT})$ at $f_p = 6.0$ GHz with various P. (d) $f_p/2$ dependence of the magnetic field H_{peak} where $\bar{\kappa}(P) - \bar{\kappa}(P = 800\ \text{mT})$ is maximized. The solid circles are the experimental data. The solid line in red was obtained using Eq. (1) with $\mu_0 M_s = 175$ mT.

Figure 5(d) shows the f_p dependence of H_{peak} for the Pt/YIG bilayer. This result is consistent with the magnon-polaron spin pumping scenario. We calculate the magnetic field $\mu_0 H_{mp}$ where the parametric excitation creates the magnon polarons using the uncoupled magnon and phonon dispersions: $f = 1/(2\pi)\sqrt{(Dk^2 + \gamma\mu_0 H)(Dk^2 + \gamma\mu_0 H + (1/2)\gamma\mu_0 M_s)}$ and $f = c/(2\pi)k$, where $\gamma = 1.76 \times 10^{11}$ s^{-1} T^{-1} is the gyromagnetic ratio and c is the TA-phonon sound velocity. For simplicity, we assumed the bulk dispersion relation for spin waves with $\theta_k = 45°$. By solving the coupled equations of the uncoupled magnon and phonon dispersions with $f = f_p/2$, we obtain an approximated relation between $f_p/2$ and $\mu_0 H_{mp}$

$$\mu_0 H_{mp} = \frac{1}{4\gamma}\left(-\gamma\mu_0 M_s - \frac{4Df_p^2\pi^2}{c^2} + \sqrt{16f_p^2\pi^2 + (\gamma\mu_0 M_s)^2}\right). \quad (1)$$

The solid red line in Fig. 5(d) is the $f_p/2$ dependence of $\mu_0 H_{mp}$ calculated with the TA-phonon sound velocity of a YIG film, $c = 3.9 \times 10^3$ m/s [2]. This result demonstrates that $\mu_0 H_{peak}$ is the magnetic field $\mu_0 H_{mp}$ where the parametric excitation creates the magnon polarons; the

spin pumping at $\mu_0 H_{\text{peak}}$ is driven by the parametrically excited magnon polarons (see also Ref. [37]).

The observed enhancement of the spin pumping is consistent with a model where the spin pumping is governed by the magnon lifetimes. For simplicity, we assume that the pumped spin current, or V_{ISHE}, is proportional to the total number of the parametrically excited magnons, n_k, in the YIG layer. In the YIG layer, the microwave absorption intensity P_{abs} is proportional to n_k/τ_k, where τ_k is the lifetime of the parametrically excited magnons. Thus, the spin-pumping efficiency, defined as $\kappa = V_{\text{ISHE}}/P_{\text{abs}}$, is approximately proportional to the lifetime of the magnon mode responsible for the spin pumping: $\kappa \propto \tau_k$ [53]. This indicates that the observed enhancement of κ can be induced when the lifetime of the hybridized magnon-phonon mode is longer than the purely magnonic lifetime. This interpretation of the efficient spin pumping driven by the magnon polarons is consistent with the model of the enhancement of the SSE. In the SSE, it has been shown that if the phonon lifetime is longer than that of magnons, the magnon-polaron formation leads to the enhanced SSE due to the longer lifetime of the magnon polarons [10,11].

In summary, we observed a resonant enhancement of the spin-pumping efficiency under the microwave parametric excitation. We demonstrated that the enhancement appears when the spin pumping is driven by hybridized magnon and phonon modes: magnon polarons. Because the microwave parametric pumping enables the selective excitation of the dominant magnon mode with a narrow range of wave vectors and energies, the spin pumping can be tuned to be purely driven by the magnon polarons. Thus, the magnon-polaron spin pumping promises to provide an essential information for fundamental understanding of the role of the magnon-phonon coupling in spintronic and magnonic phenomena.

This work was supported by JSPS KAKENHI Grants No. 26220604 and No. 26103004, the Asahi Glass Foundation, and Spintronics Research Network of Japan.

*To whom all correspondence should be addressed.
ando@appi.keio.ac.jp

[1] C. Kittel, Phys. Rev. **110**, 836 (1958).
[2] A. G. Gurevich and G. A. Melkov, *Magnetization Oscillations and Waves* (CRC Press, New York, 1996).
[3] A. Kamra, H. Keshtgar, P. Yan, and G. E. W. Bauer, Phys. Rev. B **91**, 104409 (2015).
[4] K. Shen and G. E. W. Bauer, Phys. Rev. Lett. **115**, 197201 (2015).
[5] J.-J. Song, P. Klein, R. Wadsack, M. Selders, S. Mroczkowski, and R. Chang, J. Opt. Soc. Am. **63**, 1135 (1973).
[6] F. Körmann, B. Grabowski, B. Dutta, T. Hickel, L. Mauger, B. Fultz, and J. Neugebauer, Phys. Rev. Lett. **113**, 165503 (2014).
[7] J. Oh, M. D. Le, H.-H. Nahm, H. Sim, J. Jeong, T. G. Perring, H. Woo, K. Nakajima, S. Ohira-Kawamura, Z. Yamani *et al.*, Nat. Commun. **7**, 13146 (2016).
[8] H. Man, Z. Shi, G. Xu, Y. Xu, X. Chen, S. Sullivan, J. Zhou, K. Xia, J. Shi, and P. Dai, Phys. Rev. B **96**, 100406 (2017).
[9] N. Ogawa, W. Koshibae, A. J. Beekman, N. Nagaosa, M. Kubota, M. Kawasaki, and Y. Tokura, Proc. Natl. Acad. Sci. U.S.A. **112**, 8977 (2015).
[10] T. Kikkawa, K. Shen, B. Flebus, R. A. Duine, K.-i. Uchida, Z. Qiu, G. E. W. Bauer, and E. Saitoh, Phys. Rev. Lett. **117**, 207203 (2016).
[11] B. Flebus, K. Shen, T. Kikkawa, K.-i. Uchida, Z. Qiu, E. Saitoh, R. A. Duine, and G. E. W. Bauer, Phys. Rev. B **95**, 144420 (2017).
[12] D. A. Bozhko, P. Clausen, G. A. Melkov, V. S. L'vov, A. Pomyalov, V. I. Vasyuchka, A. V. Chumak, B. Hillebrands, and A. A. Serga, Phys. Rev. Lett. **118**, 237201 (2017).
[13] J. Holanda, D. S. Maior, A. Azevedo, and S. M. Rezende, Nat. Phys. **14**, 500 (2018).
[14] L. J. Cornelissen, K. Oyanagi, T. Kikkawa, Z. Qiu, T. Kuschel, G. E. W. Bauer, B. J. van Wees, and E. Saitoh, Phys. Rev. B **96**, 104441 (2017).
[15] K. An, K. S. Olsson, A. Weathers, S. Sullivan, X. Chen, X. Li, L. G. Marshall, X. Ma, N. Klimovich, J. Zhou, L. Shi, and X. Li, Phys. Rev. Lett. **117**, 107202 (2016).
[16] M. Agrawal, V. I. Vasyuchka, A. A. Serga, A. D. Karenowska, G. A. Melkov, and B. Hillebrands, Phys. Rev. Lett. **111**, 107204 (2013).
[17] S. Mizukami, Y. Ando, and T. Miyazaki, Phys. Rev. B **66**, 104413 (2002).
[18] Y. Tserkovnyak, A. Brataas, and G. E. W. Bauer, Phys. Rev. Lett. **88**, 117601 (2002).
[19] B. Heinrich, Y. Tserkovnyak, G. Woltersdorf, A. Brataas, R. Urban, and G. E. W. Bauer, Phys. Rev. Lett. **90**, 187601 (2003).
[20] A. Azevedo, L. H. Vilela-Leão, R. L. Rodriguez-Suarez, A. B. Oliveira, and S. M. Rezende, J. Appl. Phys. **97**, 10C715 (2005).
[21] E. Saitoh, M. Ueda, H. Miyajima, and G. Tatara, Appl. Phys. Lett. **88**, 182509 (2006).
[22] M. V. Costache, M. Sladkov, S. M. Watts, C. H. van der Wal, and B. J. van Wees, Phys. Rev. Lett. **97**, 216603 (2006).
[23] K. Ando, Y. Kajiwara, S. Takahashi, S. Maekawa, K. Takemoto, M. Takatsu, and E. Saitoh, Phys. Rev. B **78**, 014413 (2008).
[24] O. Mosendz, J. E. Pearson, F. Y. Fradin, G. E. W. Bauer, S. D. Bader, and A. Hoffmann, Phys. Rev. Lett. **104**, 046601 (2010).
[25] O. Mosendz, V. Vlaminck, J. E. Pearson, F. Y. Fradin, G. E. W. Bauer, S. D. Bader, and A. Hoffmann, Phys. Rev. B **82**, 214403 (2010).
[26] B. Heinrich, C. Burrowes, E. Montoya, B. Kardasz, E. Girt, Y.-Y. Song, Y. Sun, and M. Wu, Phys. Rev. Lett. **107**, 066604 (2011).
[27] A. Azevedo, L. H. Vilela-Leão, R. L. Rodriguez-Suarez, A. F. Lacerda Santos, and S. M. Rezende, Phys. Rev. B **83**, 144402 (2011).
[28] H. Kurebayashi, O. Dzyapko, V. E. Demidov, D. Fang, A. J. Ferguson, and S. O. Demokritov, Appl. Phys. Lett. **99**, 162502 (2011).

[29] C. W. Sandweg, Y. Kajiwara, A. V. Chumak, A. A. Serga, V. I. Vasyuchka, M. B. Jungfleisch, E. Saitoh, and B. Hillebrands, Phys. Rev. Lett. **106**, 216601 (2011).
[30] M. Weiler, M. Althammer, M. Schreier, J. Lotze, M. Pernpeintner, S. Meyer, H. Huebl, R. Gross, A. Kamra, J. Xiao, Y.-T. Chen, H. Jiao, G. E. W. Bauer, and S. T. B. Goennenwein, Phys. Rev. Lett. **111**, 176601 (2013).
[31] Y. Sun, H. Chang, M. Kabatek, Y.-Y. Song, Z. Wang, M. Jantz, W. Schneider, M. Wu, E. Montoya, B. Kardasz, B. Heinrich, S. G. E. te Velthuis, H. Schultheiss, and A. Hoffmann, Phys. Rev. Lett. **111**, 106601 (2013).
[32] S. M. Rezende, R. L. Rodríguez-Suárez, and A. Azevedo, Phys. Rev. B **88**, 014404 (2013).
[33] S. A. Manuilov, C. H. Du, R. Adur, H. L. Wang, V. P. Bhallamudi, F. Y. Yang, and P. C. Hammel, Appl. Phys. Lett. **107**, 042405 (2015).
[34] Y. Tserkovnyak, A. Brataas, G. E. W. Bauer, and B. I. Halperin, Rev. Mod. Phys. **77**, 1375 (2005).
[35] T. Kikkawa, K.-i. Uchida, S. Daimon, Z. Qiu, Y. Shiomi, and E. Saitoh, Phys. Rev. B **92**, 064413 (2015).
[36] R. Iguchi, K. Ando, R. Takahashi, T. An, E. Saitoh, and T. Sato, Jpn. J. Appl. Phys. **51**, 103004 (2012).
[37] See Supplemental Material at http://link.aps.org/supplemental/10.1103/PhysRevLett.121.237202 for a detailed description of magnetostatic spin waves, nonlinear ferromagnetic resonance, three-magnon process, temperature dependence of spin-pumping efficiency, and spin pumping under oblique pumping, which includes Refs. [38–44].
[38] R. W. Damon and J. Eshbach, J. Phys. Chem. Solids **19**, 308 (1961).
[39] Y. Kajiwara, K. Harii, S. Takahashi, J. Ohe, K. Uchida, M. Mizuguchi, H. Umezawa, H. Kawai, K. Ando, K. Takanashi, S. Maekawa, and E. Saitoh, Nature (London) **464**, 262 (2010).
[40] C. W. Sandweg, Y. Kajiwara, K. Ando, E. Saitoh, and B. Hillebrands, Appl. Phys. Lett. **97**, 252504 (2010).
[41] S. Dushenko, Y. Higuchi, Y. Ando, T. Shinjo, and M. Shiraishi, Appl. Phys. Express **8**, 103002 (2015).
[42] M. B. Jungfleisch, A. V. Chumak, A. Kehlberger, V. Lauer, D. H. Kim, M. C. Onbasli, C. A. Ross, M. Kläui, and B. Hillebrands, Phys. Rev. B **91**, 134407 (2015).
[43] J. S. Plant, J. Phys. C **10**, 4805 (1977).
[44] Y. Liu and C. Patton, J. Appl. Phys. **53**, 5116 (1982).
[45] V. S. L'vov, *Wave Turbulence Under Parametric Excitation* (Springer-Verlag, Berlin, 1994).
[46] M. Fukami, Y. Tateno, K. Sekiguchi, and K. Ando, Phys. Rev. B **93**, 184429 (2016).
[47] W. D. Wilber, J. G. Booth, C. E. Patton, G. Srinivasan, and R. W. Cross, J. Appl. Phys. **64**, 5477 (1988).
[48] G. Wiese, P. Kabos, and C. E. Patton, Phys. Rev. B **51**, 15085 (1995).
[49] H. Kurebayashi, O. Dzyapko, V. E. Demidov, D. Fang, A. J. Ferguson, and S. O. Demokritov, Nat. Mater. **10**, 660 (2011).
[50] V. Castel, N. Vlietstra, B. J. van Wees, and J. B. Youssef, Phys. Rev. B **86**, 134419 (2012).
[51] S. C. Guerreiro and S. M. Rezende, Phys. Rev. B **92**, 214437 (2015).
[52] C. W. Sandweg, M. B. Jungfleisch, V. I. Vasyuchka, A. A. Serga, P. Clausen, H. Schultheiss, B. Hillebrands, A. Kreisel, and P. Kopietz, Rev. Sci. Instrum. **81**, 073902 (2010).
[53] H. Sakimura, T. Tashiro, and K. Ando, Nat. Commun. **5**, 5730 (2014).